Composition dependence of spin orbit torque in Pt1 xMnx/CoFeB heterostructures

Composition dependence of spin–orbit torque in $Pt_{1-x}Mn_x$/CoFeB heterostructures $\textcircled{\tiny EP}$

K. Vihanga De Zoysa, ⓘ Samik DuttaGupta, Ryuichi Itoh, Yutaro Takeuchi, ⓘ Hideo Ohno, and ⓘ Shunsuke Fukami

COLLECTIONS

EP   This paper was selected as an Editor's Pick

**View Online**   **Export Citation**   **CrossMark**

ARTICLES YOU MAY BE INTERESTED IN

Electrical control of antiferromagnets for the next generation of computing technology
Applied Physics Letters **117**, 010501 (2020); https://doi.org/10.1063/5.0013917

Spintronics with compensated ferrimagnets
Applied Physics Letters **116**, 110501 (2020); https://doi.org/10.1063/1.5144076

Study of the perpendicular magnetic anisotropy, spin–orbit torque, and Dzyaloshinskii–Moriya interaction in the heavy metal/CoFeB bilayers with $Ir_{22}Mn_{78}$ insertion
Applied Physics Letters **116**, 242407 (2020); https://doi.org/10.1063/5.0006138
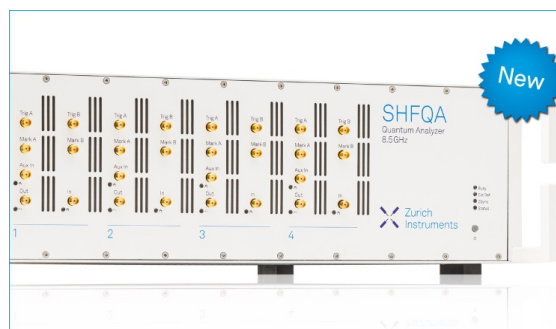
Composition dependence of spin−orbit torque in $Pt_{1−x}Mn_x$/CoFeB heterostructures (EP)

View Online   Export Citation   CrossMark

K. Vihanga De Zoysa,[1] Samik DuttaGupta,[1,2,3,a] (iD) Ryuichi Itoh,[1] Yutaro Takeuchi,[1] Hideo Ohno,[1,2,3,4,5] (iD)
and Shunsuke Fukami[1,2,3,4,5] (iD)

AFFILIATIONS

[1]Laboratory for Nanoelectronics and Spintronics, Research Institute of Electrical Communication, Tohoku University, 2-1-1 Katahira,
 Aoba-ku, Sendai 980-8577, Japan
[2]Center for Science and Innovation in Spintronics, Tohoku University, 2-1-1 Katahira, Aoba-ku, Sendai 980-8577, Japan
[3]Center for Spintronics Research Network, Tohoku University, 2-1-1 Katahira, Aoba-ku, Sendai 980-8577, Japan
[4]Center for Innovative Integrated Electronic Systems, Tohoku University, 468-1 Aramaki Aza Aoba, Aoba-ku, Sendai 980-0845, Japan
[5]WPI-Advanced Institute for Materials Research, Tohoku University, 2–1–1 Katahira, Aoba-ku, Sendai 980-8577, Japan

[a]Author to whom correspondence should be addressed: sdg@riec.tohoku.ac.jp

ABSTRACT

We investigate spin–orbit torques (SOTs) in heterostructures with $Pt_{1−x}Mn_x$ alloy and CoFeB as a function of Mn composition (x) by using an extended harmonic Hall measurement. Slonczewski-like and field-like SOT efficiencies (ξ_{SL} and ξ_{FL}) show non-monotonic variation and a different trend with respect to x, and considerably large ξ_{SL} up to 0.21 is obtained at $x = 0.20$. Compared to the x dependence of longitudinal resistivity, the Slonczewski-like SOT in the low x region is mainly attributed to an intrinsic spin-Hall mechanism, whereas a non-monotonic variation in the higher x region suggests the presence of additional factors. The present findings deliver useful clues to understand the physics behind SOT generation in antiferromagnetic heterostructures and offer a route to realize efficient devices.

Published under license by AIP Publishing. https://doi.org/10.1063/5.0011448

The utilization of current-induced spin–orbit torques (SOTs) in magnetic heterostructures has recently gained enormous importance owing to their potential in future spintronic devices.[1–8] Three-terminal non-volatile spintronic devices utilizing SOT-induced magnetization switching achieve fast and reliable operation, showing promise for integrated-circuit applications.[5–8] Conventional device geometries utilize non-magnet (NM)/ferromagnet (FM) structures, where the current passing through the stack gives rise to the Slonczewski-like (SL) and field-like (FL) SOTs, allowing magnetization reversal.[2,3,5] The search for NM materials exhibiting large SOT efficiencies has so far mainly focused on $5d$ transition metal elements owing to their strong spin–orbit coupling.[9–18] However, in a practical scenario, manipulation of magnetization in the NM/FM heterostructure requires a unipolar magnetic field to determine the switching direction, posing a challenge for applications. Recent studies tackled this unfavorable requirement using antiferromagnet (AFM)/FM structures, where an AFM plays a dual role, generator of SOTs, and source of symmetry-breaking magnetic fields originating from interfacial exchange bias.[19,20] Moreover, experimental results on a heterostructure with antiferromagnetic $Pt_{0.38}Mn_{0.62}$ showed an analog-like switching,[19,21]

which is attractive for neuromorphic applications as well.[22,23] Two prerequisites for efficient field-free magnetization switching are large SOTs and an exchange bias field in AFM/FM heterostructures. Some previous experimental results on Mn-based binary AFM/FM structures have demonstrated appreciable SOT magnitude, tunable with respect to the crystalline orientation, Mn composition, and magnetic order.[24–28] PtMn is known to show the largest SOT among the Mn-based AFMs.[24] We previously studied the SOT in PtMn/FM (FM = [Co/Ni][29] or CoFeB[30]) heterostructures with a specific PtMn composition and found that the SL-SOT is mainly attributed to the spin Hall effect (SHE) of PtMn. However, the underlying factors for the SOT, e.g., the dominant role of intrinsic/extrinsic mechanisms in the SHE, and the effect of structural and magnetic order have not been investigated well. Here, we study SOTs in PtMn/CoFeB structures with various Mn compositions. In order to get insights into the origin of SOTs in this system, the results are analyzed with respect to the variations in longitudinal resistivity and expected magnetic order as a function of Mn composition.

We utilize Si/SiO_2 sub./Ta(3)/Ru(1.5)/$Pt_{1−x}Mn_x$(10)/ $(Co_{25}Fe_{75})_{0.75}B_{0.25}$(1.8)/MgO(1.5)/Ru(1) structures ($Pt_{1−x}Mn_x$/CoFeB,

hereafter) [Fig. 1(a)], which are prepared by DC and RF magnetron sputtering (numbers in parentheses are nominal thicknesses in nm). Mn composition x is varied as 0, 0.11, 0.20, 0.27, 0.39, 0.51, 0.57, 0.70, and 0.78 by co-sputtering of Pt and $Pt_{0.18}Mn_{0.82}$ targets. The composition of the PtMn layer is determined by inductively coupled plasma mass spectrometry. The samples are annealed at $300\,°C$ for 2 h in the presence of an in-plane magnetic field of 1.2 T, similar to our previous studies.[19,29,30] Out-of-plane x-ray diffraction (XRD) spectra indicate a textured polycrystalline orientation of the PtMn layer along the (111) direction.[31] Figures 1(b) and 1(c) show the magnetization (m-H) curve of annealed blanket films for the applied field (H) along the in-plane and out-of-plane directions, respectively. The in-plane easy axis, which is necessary for the extended harmonic Hall measurement, is confirmed for all $Pt_{1-x}Mn_x$/CoFeB structures studied here. We also observe a decrease in areal magnetic moment m with increasing x, probably due to a slight intermixing at the PtMn/CoFeB interface, which increases with x, and/or proximity-induced moments in PtMn, which decrease with x.[32] Besides, m-H measurements indicate exchange bias fields of ≈ 17 and 3 mT for Mn concentrations of $x = 0.51$ and 0.57, respectively, while they are virtually zero away from the equiatomic composition. The resistivities (ρ) of the $Pt_{1-x}Mn_x$ layers are determined by measuring sheet resistance on a series of blanket films.[19] The current flow ratio, which is used to calculate the Oersted field (H_{Oe})[18,30] and SOT generation efficiency later, is derived from the obtained ρ of each layer. Figure 1(d) shows the variation of ρ for PtMn as a function of x. We observe a linear increase in ρ up to $x \approx 0.27$, followed by a non-monotonic variation for higher Mn compositions; the trend is roughly consistent with a previous report.[33] This result will be used to discuss the origin of SOT later.

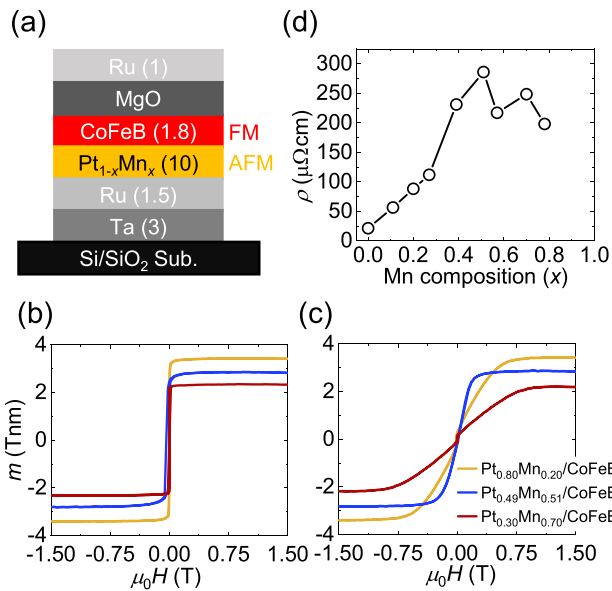The deposited films are then patterned into $10 \times 50\,\mu m^2$ Hall bar devices by photolithography and Ar-ion milling. We use an extended harmonic Hall method to quantify the SL and FL components of SOTs, free from thermal effects.[15,17] Figure 2(a) shows the schematic diagram of the harmonic Hall measurement setup. AC of frequency 11 Hz is applied to the Hall bar structures while rotating an external magnetic field (H_{ext}) with a constant magnitude along the azimuthal plane (angle φ between H_{ext} and current is measured from the x-axis). We measure the first (R_ω) and second ($R_{2\omega}$) harmonic Hall resistance using a lock-in technique. We obtain SL (H_{SL}) and FL (H_{FL}) components of SOT-induced effective fields by fitting R_ω and $R_{2\omega}$ vs φ. Prior to the harmonic Hall measurement, we determine the anomalous Hall resistance coefficient (R_{AHE}) and effective anisotropy field (H_K^{eff}) for all the samples, which are required for the determination of H_{SL} and H_{FL}. Figure 2(b) shows typical experimental data of Hall resistance (R_{Hall}) vs out-of-plane field H_z under the application of DC for a $Pt_{0.70}Mn_{0.30}$/CoFeB structure. A linear fit to the high field region yields R_{AHE}, while that from low field regions yields H_K^{eff}, as illustrated in the figure.

Now, we show the results for the extended harmonic Hall measurements. Figures 3(a) and 3(b) show the measured R_ω and $R_{2\omega}$ as a function of φ for PtMn/CoFeB with various x values under an applied $\mu_0 H_{ext} = 200$ mT (μ_0 is the permeability in free space). Owing to the in-plane easy-axis along with negligible anisotropy in the film plane, R_ω can be expressed as[15,17,30]

$$R_\omega = R_{PHE} \sin 2\varphi, \qquad (1)$$

where R_{PHE} is the planar Hall resistance coefficient. Black curves in Fig. 3(a) denote the fitting of Eq. (1) to the experimental results. R_{PHE} obtained from fitting is later used for the determination of H_{SL} and H_{FL}. Under the SHE scenario, the application of charge current along the x-direction results in a transverse spin accumulation at the PtMn/FM interface, leading to current-induced SOTs, as shown previously in $Pt_{0.38}Mn_{0.62}$/FM structures.[29,30] The resulting modulation of the magnetization direction by SOTs manifests in a harmonic dependence of $R_{2\omega}$, expressed as[15,17,30]

$$R_{2\omega} = -\left(R_{AHE}\frac{H_{SL}}{H_{ext} - H_K^{eff}} + R_{\triangle T}^0\right)\cos\varphi$$
$$+ 2R_{PHE}\left(2\cos^3\varphi - \cos\varphi\right)\frac{H_{FL} + H_{Oe}}{H_{ext}}, \qquad (2)$$

where $R_{\triangle T}^0$ is the second harmonic Hall coefficient originating from thermal effects. Figure 3(b) shows the raw data and fitting curves with
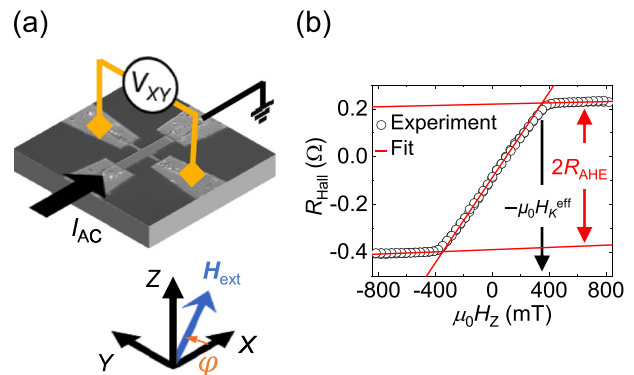

FIG. 1. (a) Schematic representation of the stack structure and (b) and (c) areal magnetic moment (m) vs applied magnetic field for in-plane and out-of-plane configurations, respectively, for Mn compositions $x = 0.20$, 0.51, and 0.70. (d) Longitudinal resistivity (ρ) of $Pt_{1-x}Mn_x$ as a function of Mn composition (x).

FIG. 2. (a) Schematic representation of the experimental setup. (b) Hall resistance (R_{Hall}) vs out-of-plane magnetic field (H_Z) for the $Pt_{0.70}Mn_{0.30}$/CoFeB structure.
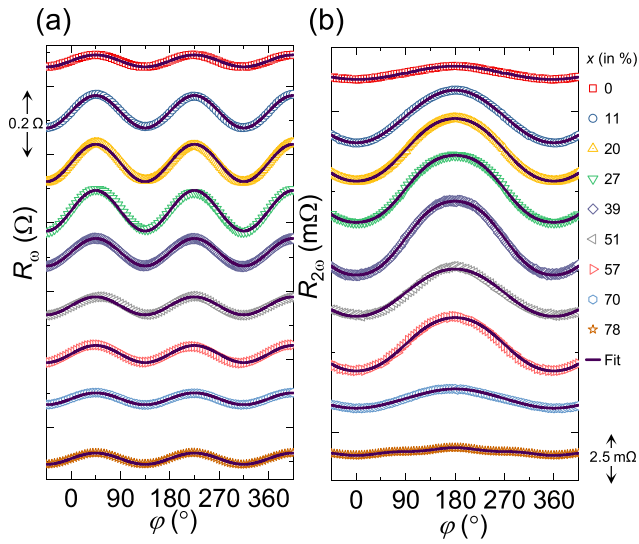
FIG. 3. Azimuthal angle (φ) dependence of (a) first (R_ω) and (b) second ($R_{2\omega}$) harmonic Hall resistance for $Pt_{1-x}Mn_x$/CoFeB ($0 \leq x \leq 0.78$) structures. Solid lines denote fitting to the experimental data using Eqs. (1) and (2). Figure legends (right) denote the Mn composition x (in %) for the $Pt_{1-x}Mn_x$/CoFeB structures, investigated in this study.

FIG. 4. Mn composition (x) dependence of (a) ξ_{SL} and (b) ξ_{FL} component of SOT efficiencies for $Pt_{1-x}Mn_x$/CoFeB structures. Data points (error bars) in (a) and (b) are obtained as the average (standard deviation) of $\xi_{SL,FL}$ from measurements of five identical devices.

Eq. (2). We carry out similar experiments for different magnitudes of H_{ext} to eliminate $R^0_{\triangle T}$. We obtain H_{SL} from a linear fitting of the H_{ext} dependence of the coefficient of the first term in Eq. (2), while H_{FL} is obtained from the coefficient of the second term for maximum applied $\mu_0 H_{ext}$ (= 300 mT).

To quantify the strength of SOTs irrespective of material parameters, we introduce a dimensionless quantity $\xi_{SL(FL)}$ characterizing the efficiency of SOT generation, expressed as[16,17]

$$\xi_{SL(FL)} = \frac{2eH_{SL(FL)}M_S t}{\hbar J_{PtMn}}, \qquad (3)$$

where e is the elementary charge, $\hbar$ is the Dirac constant, J_{PtMn} is the current density in the $Pt_{1-x}Mn_x$ layer determined from the current flow ratio, M_S is the spontaneous magnetization of FM, and t is the thickness of the FM. Note that ξ_{SL} corresponds to the effective spin Hall angle under an assumption that the SHE is responsible for SOT. Figures 4(a) and 4(b) summarize the x dependence of ξ_{SL} and ξ_{FL}, respectively. We measure five identical devices for each x, and the average and standard deviation for them are shown by the plot and error bar. We observe a non-monotonic variation for both $\xi_{SL(FL)}$ with x, and their trends are different from each other. At $x = 0$, i.e., pure Pt, $\xi_{SL(FL)} = 0.088 \pm 0.001$ (0.007 ± 0.001), comparable to previous results for Pt.[9,16] An increase in x increases ξ_{SL} up to 0.208 ± 0.001 at $x = 0.20$ and then decreases gradually with a further increase in x. ξ_{FL} shows a similar behavior, but its maximum is located at around the equiatomic composition. The maximum values of ξ_{SL} for $Pt_{0.8}Mn_{0.2}$/CoFeB are substantially larger than those of most of the commonly known $5d$ transition metal elements (e.g., Pt and Ta).[2,3,9,11–17] These results indicate the presence of additional factors beyond the spin–orbit coupling of the heavy elements on the strength of SOTs in Mn-based alloys.

Finally, we discuss the possible origins for the observed variation of SOTs with x and considerably large ξ_{SL}. Under the SHE scenario,
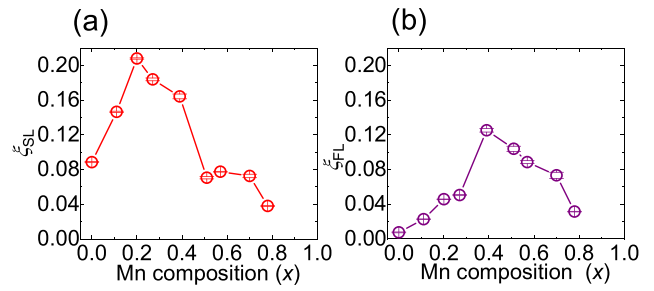
the spin-charge conversion mechanism possesses intrinsic contributions arising from the Berry curvature associated with the electronic band structure and extrinsic contributions originating from spin-dependent skew and side-jump scattering. Accordingly, ξ_{SL} can be expressed as[34] $\sigma_{SH} \rho_{el} + \xi^{SS}$, where ρ_{el} represents the bulk electrical resistivity of the material, σ_{SH} denotes the spin-Hall conductivity from the intrinsic and side-jump mechanisms, and ξ^{SS} represents the ρ_{el}-independent contribution from skew scattering. Note that the intrinsic mechanism could originate not only from the spin–orbit coupling of heavy elements but also from the local spin structure.[27] Our results in the low x (≤ 0.2) regime show a mutual increase in ρ [Fig. 1(d)] and ξ_{SL} [Fig. 4(a)]. This rules out any dominant contribution from ξ^{SS} and suggests the ρ_{el}-dependent part to be mainly responsible for ξ_{SL}. We estimate $\sigma_{SH} \approx 1784\ \Omega^{-1}$ cm^{-1}, in this regime, comparable to the previous results for intrinsic spin Hall conductivity of Pt.[35–37] Interestingly, ξ_{FL} also shows a similar behavior with a much smaller magnitude, implying a common origin. For $x > 0.2$, ρ increases further, while ξ_{SL} decreases, indicating the presence of additional factors. We speculate that this progressive decrease in ξ_{SL} may be associated with magnetic order,[25,27,28] the presence of the pseudo-gap at the Fermi level[37] at a high Mn-composition, and/or the influence of intermixing/induced moments at the PtMn/CoFeB interface. Note that the emergence of collinear or non-collinear antiferromagnetic order can modify spin–orbit coupling,[26–28] while the presence of the gap at E_F can modify the band structure,[38] both of which can influence SOT efficiencies. The complicated behavior of ξ_{FL} may be related to the Rashba–Edelstein effects and/or spin-dependent scattering effects.[39–41] Nevertheless, our results indicate a possibility to enhance SOTs in metallic AFM/FM structures and call for further studies on SOT generation in AFM/FM systems.

In summary, we quantified the composition dependence of SOTs in $Pt_{1-x}Mn_x$/CoFeB using an extended harmonic Hall measurement. We observed a large ξ_{SL} (= 0.21) for $Pt_{0.80}Mn_{0.20}$ and a non-monotonic variation of SOTs with x. The large SOT efficiency is qualitatively found to arise from an intrinsic mechanism, while the non-monotonic variation of SOTs with x suggests the presence of additional factors that may be associated with magnetic order or modification of the band structure. The present experimental results provide considerable insights into the origin of SOTs in AFM/FM and suggest a possible route toward enhancing SOTs for future spintronic devices.

DATA AVAILABILITY

The data that support the findings of this study are available from the corresponding author upon reasonable request.

REFERENCES

[1] I. M. Miron, K. Garello, G. Gaudin, P.-J. Zermatten, M. V. Costache, S. Auffret, S. Bandiera, B. Rodmacq, A. Schuhl, and P. Gambardella, Nature **476**, 189 (2011).

[2] L. Liu, C.-F. Pai, Y. Li, H. W. Tseng, D. C. Ralph, and R. A. Buhrman, Science **336**, 555 (2012).

[3] L. Liu, O. J. Lee, T. J. Gudmundsen, D. C. Ralph, and R. A. Buhrman, Phys. Rev. Lett. **109**, 096602 (2012).

[4] S. Fukami, T. Anekawa, C. Zhang, and H. Ohno, Nat. Nanotechnol. **11**, 621 (2016).

[5] K. Garello, C. O. Avci, I. M. Miron, M. Baumgartner, A. Ghosh, S. Auffret, O. Boulle, G. Gaudin, and P. Gambardella, Appl. Phys. Lett. **105**, 212402 (2014).

[6] S. Fukami, T. Anekawa, A. Ohkawara, C. Zhang, and H. Ohno, in *IEEE Symposium on VLSI Technology*, T06-05 (IEEE, 2016).

[7] S. Shi, Y. Ou, S. V. Aradhya, D. C. Ralph, and R. A. Buhrman, Phys. Rev. Appl. **9**, 011002 (2018).

[8] S. Fukami and H. Ohno, Jpn. J. Appl. Phys., Part 1 **56**, 0802A1 (2017).

[9] L. Liu, T. Moriyama, D. C. Ralph, and R. A. Buhrman, Phys. Rev. Lett. **106**, 036601 (2011).

[10] T. Suzuki, S. Fukami, N. Ishiwata, M. Yamanouchi, S. Ikeda, N. Kasai, and H. Ohno, Appl. Phys. Lett. **98**, 142505 (2011).

[11] K. Garello, I. M. Miron, C. O. Avci, F. Freimuth, Y. Mokrousov, S. Blügel, S. Auffret, O. Boulle, G. Gaudin, and P. Gambardella, Nat. Nanotechnol. **8**, 587 (2013).

[12] J. Kim, J. Sinha, M. Hayashi, M. Yamanouchi, S. Fukami, T. Suzuki, S. Mitani, and H. Ohno, Nat. Mater. **12**, 240 (2013).

[13] C. Zhang, M. Yamanouchi, H. Sato, S. Fukami, S. Ikeda, F. Matsukura, and H. Ohno, Appl. Phys. Lett. **103**, 262407 (2013).

[14] X. Fan, J. Wu, Y. Chen, M. J. Jerry, H. Zhang, and J. Q. Xiao, Nat. Commun. **4**, 1799 (2013).

[15] C. O. Avci, K. Garello, M. Gabureac, A. Ghosh, A. Fuhrer, S. F. Alvarado, and P. Gambardella, Phys. Rev. B **90**, 224427 (2014).

[16] C.-F. Pai, Y. Ou, L. H. Vilela-Leão, D. C. Ralph, and R. A. Buhrman, Phys. Rev. B **92**, 064426 (2015).

[17] Y.-C. Lau and M. Hayashi, Jpn. J. Appl. Phys., Part 1 **56**, 0802B5 (2017).

[18] Y. Takeuchi, C. Zhang, A. Okada, H. Sato, S. Fukami, and H. Ohno, Appl. Phys. Lett. **112**, 192408 (2018).

[19] S. Fukami, C. Zhang, S. DuttaGupta, A. Kurenkov, and H. Ohno, Nat. Mater. **15**, 535 (2016).

[20] Y. W. Oh, S. H. Chris Baek, Y. M. Kim, H. Y. Lee, K. D. Lee, C. G. Yang, E. S. Park, K. S. Lee, K. W. Kim, G. Go, J. R. Jeong, B. C. Min, H. W. Lee, K. J. Lee, and B. G. Park, Nat. Nanotechnol. **11**, 878 (2016).

[21] A. Kurenkov, C. Zhang, S. DuttaGupta, S. Fukami, and H. Ohno, Appl. Phys. Lett. **110**, 092410 (2017).

[22] W. A. Borders, H. Akima, S. Fukami, S. Moriya, S. Kurihara, Y. Horio, S. Sato, and H. Ohno, Appl. Phys. Express **10**, 013007 (2017).

[23] A. Kurenkov, S. DuttaGupta, C. Zhang, S. Fukami, Y. Horio, and H. Ohno, Adv. Mater. **31**, 1900636 (2019).

[24] W. Zhang, M. B. Jungfleisch, W. Jiang, J. E. Pearson, A. Hoffmann, F. Freimuth, and Y. Mokrousov, Phys. Rev. Lett. **113**, 196602 (2014).

[25] W. Zhang, M. B. Jungfleisch, F. Freimuth, W. Jiang, J. Sklenar, J. E. Pearson, J. B. Ketterson, Y. Mokrousov, and A. Hoffmann, Phys. Rev. B **92**, 144405 (2015).

[26] V. Tshitoyan, C. Ciccarelli, A. P. Mihai, M. Ali, A. C. Irvine, T. A. Moore, T. Jungwirth, and A. J. Ferguson, Phys. Rev. B **92**, 214406 (2015).

[27] W. Zhang, W. Han, S.-H. Yang, Y. Sun, Y. Zhang, B. Yan, and S. S. P. Parkin, Sci. Adv. **2**, e1600759 (2016).

[28] J. Zhou, X. Wang, Y. Liu, J. Yu, H. Fu, L. Liu, S. Chen, J. Deng, W. Lin, X. Shu, H. Y. Yoong, T. Hong, M. Matsuda, P. Yang, S. Adams, B. Yan, X. Han, and J. Chen, Sci. Adv. **5**, eaau6696 (2019).

[29] S. DuttaGupta, T. Kanemura, C. Zhang, A. Kurenkov, S. Fukami, and H. Ohno, Appl. Phys. Lett. **111**, 182412 (2017).

[30] R. Itoh, Y. Takeuchi, S. DuttaGupta, S. Fukami, and H. Ohno, Appl. Phys. Lett. **115**, 242404 (2019).

[31] S. DuttaGupta, R. Itoh, S. Fukami, and H. Ohno, Appl. Phys. Lett. **113**, 202404 (2018).

[32] W. A. Borders, S. Fukami, and H. Ohno, IEEE Trans. Magn. **53**, 1 (2017).

[33] S. Honda, M. Nawate, and T. Norikane, J. Magn. Magn. Mater. **220**, 85 (2000).

[34] Y. Niimi and Y. Otani, Rev. Prog. Phys. **78**, 124501 (2015).

[35] E. Sagasta, Y. Omori, M. Isasa, M. Gradhand, L. E. Hueso, Y. Niimi, Y. Otani, and F. Casanova, Phys. Rev. B **94**, 060412(R) (2016).

[36] T. Tanaka, H. Kontani, M. Naito, D. S. Hirashima, K. Yamada, and J. Inoue, Phys. Rev. B **77**, 165117 (2008).

[37] L. Wang, R. J. H. Wesselink, Y. Liu, Z. Yuan, K. Xia, and P. J. Kelly, Phys. Rev. Lett. **116**, 196602 (2016).

[38] R. Y. Umetsu, K. Fukamichi, and A. Sakuma, Mater. Trans. **47**, 2 (2006).

[39] P. M. Haney, H.-W. Lee, K.-J. Lee, A. Manchon, and M. D. Stiles, Phys. Rev. B **87**, 174411 (2013).

[40] Y. Ou, C.-F. Pai, S. Shi, D. C. Ralph, and R. A. Buhrman, Phys. Rev. B **94**, 140414(R) (2016).

[41] A. Manchon, J. Zelezny, I. M. Miron, T. Jungwirth, J. Sinova, A. Thiaville, K. Garello, and P. Gambardella, Rev. Mod. Phys. **91**, 035004 (2019).